Design and Development of a Spherical 5-Bar Thumb Exoskeleton Mechanism for Poststroke Rehabilitation

Vishwanath D. Ketkar[1]
Department of Electrical Engineering,
University of Idaho,
Moscow, ID 83844-0902
e-mail: ketk4164@vandals.uidaho.edu

Eric T. Wolbrecht
Department of Mechanical Engineering,
University of Idaho,
Moscow, ID 83844-0902
e-mail: ewolbrec@uidaho.edu

Joel C. Perry
Department of Mechanical Engineering,
University of Idaho,
Moscow, ID 83844-0902
e-mail: jperry@uidaho.edu

Andria Farrens
Department of Biomedical Engineering,
University of California,
Irvine, CA 92697
e-mail: farrensa@uci.edu

This paper presents the kinematic design and development of a two degree-of-freedom (2DOF) spherical 5-bar thumb exoskeleton to augment the finger individuating grasp exercise robot (FINGER) rehabilitation robot, which assists the index and middle fingers individually in naturalistic grasping. The thumb module expands the capabilities of FINGER, allowing for broader proprioceptive training and assessment of hand function. The design process started by digitizing thumb-grasping motions to the index and the middle fingers separately, recorded from multiple healthy subjects utilizing a motion capture system. Fitting spheres to trajectory data of each subject allowed normalization of all subjects' data to a common center and radius. A two-revolute joint serial-chain mechanism was synthesized (intermediate optimization step) to reach the normalized trajectories. Next, the two resulting grasping trajectories were spatially sampled as targets for the 2DOF spherical 5-bar synthesis. Optimization of the spherical 5-bar included symmetry constraints and cost-function penalties for poor manipulability. The resulting exoskeleton assists both flexion/extension and abduction/adduction of the thumb enabling a wide range of motions. Consistent with FINGER, the parallel structure of the spherical 5-bar places the actuators at the base of the module, allowing for desirable characteristics, including high backdrivability, high controllable bandwidth, and low mechanical impedance. The mechanical design was developed from the kinematic solution, including an adjustable thumb cuff to accommodate different hand sizes. Fit and function of the device were tested on multiple subjects, including survivors of stroke. A proportional-derivative force controller with gravity and friction compensation was implemented to reduce resistance to motion during subject testing. [DOI: 10.1115/1.4056864]

Introduction

Nearly 800,000 people in the U.S. suffer a stroke each year, making stroke a leading cause of long-term disability [1]. Due to an aging population and increasing survival rates, this number is projected to continue increasing over the next several decades [2]. Around 25–40% of stroke survivors suffer from minor to severe movement impairments that require rehabilitation [3]. Impairment of the hand is particularly problematic since the hand is the most frequently used upper-body part involved in activities of daily living [4]. The ability of the thumb to oppose the fingers is essential for grasp and manipulation activities, such as holding a pen, turning a doorknob, and lifting small objects. This emphasizes the need for inexpensive, targeted, and repeatable movement training of the hand, finger, and thumb. This is the need that robotic-assisted movement therapy aims to meet.

Over the last several decades, researchers have developed robotic devices for hand rehabilitation following stroke or other neurologic injury. Therapy administered with these devices has been shown to be as good as, or in some cases, marginally better than, traditional therapy for poststroke recovery [5]. Continued work is needed to determine the best design features, training approaches, and control methods for restoring thumb and finger function [6–8].

Beyond automating the physical therapy process, robotic devices can serve as a scientific instrument to investigate the poststroke recovery process and determine the factors that promote recovery. Importantly to these efforts, robots are highly repeatable and capable of a wide range of assessments (another strength of rehabilitation robotics). Researchers have used robots to investigate the role of many different factors in poststroke recovery, including motivation [9], control strategies [10], baseline capacity [11], lesion location and size [12], and neural correlates from electro-encephalography [13].

Recently, researchers have begun to develop ways to use robotic devices to assess proprioception [14–16] and investigate its role in movement recovery after stroke [17]. As the importance of the role of proprioception in neuromuscular recovery becomes clearer, efforts have been made to add proprioceptive training to poststroke, robot-assisted movement training protocols [18,19].

In recent studies, (Finger INdividuating Grasp Exercise Robot (FINGER) [20]), the robotic rehabilitation device for the index and middle finger grasping referred to in this paper, has been used to assess proprioception via the crisscross test as described in Ref. [21] that showed an age-related decline in proprioception (the crisscross test involves subjects indicating with proprioception but not vision when they perceive that their fingers have crossed as the FINGER robot moves their fingers back and forth). Of particular interest is the role of proprioception in recovery, as described in Ref. [22], which found baseline proprioception to be a significant predictor of recovery gains. To investigate this further, we sought to expand the proprioceptive assessment capabilities of FINGER by adding a thumb module and developing methods to train proprioceptive capacity in the thumb, index, and middle fingers. The design and development of the thumb module were guided by these design criteria to facilitate a poststroke movement therapy study that includes proprioception assessment and training. However, the resulting device has thumb motion capabilities beyond the scope of the movement therapy study for which it was designed, and with further development, could be

[1]Corresponding author.
Manuscript received April 19, 2022; final manuscript received January 23, 2023; published online April 17, 2023. Assoc. Editor: Elizabeth Hsiao-Wecksler.

used to provide therapy and assessment for a wide range of hand impairments in a clinic or home setting.

Background, Objectives, and Design Overview

The dexterity of the human hand enables the manipulation of objects, and the thumb is involved in over 40% of all hand functions used in activities of daily life [23,24]. The thumb's opposability, a unique feature compared to the other hand digits, is central to pinching or grasping motions. These motions are a result of the combination of not only flexion/extension motion at the metacarpophalangeal (MCP) and the carpometacarpal (CMC) joint but also the abduction/adduction motion at the CMC joint.

Robotic Devices Supporting Thumb Motion. Several robotic devices have been developed for poststroke rehabilitation of the hand that can provide intensive and repetitive movement training and assessment of impairment and function. These can be broadly classified as exoskeleton, end-effector, or glove-based devices. Exoskeleton devices are designed to mimic anatomical structure and/or movements in their kinematic design while end-effector devices have a separate kinematic structure featuring sufficient workspace to reproduce desired motions via trajectory planning. Glove-based devices typically use modified gloves as the foundational structure for sensing and actuation.

Examples of exoskeleton-type devices for hand rehabilitation are presented in Refs. [25] and [26]. Each has 4DOFs, supporting flexion–extension and abduction–adduction, allowing for opposability of the thumb during grasping and other motions. The Rutgers Master [27] is an example of an end-effector type robot, assisting flexion and extension of the CMC and the MCP joints of the thumb and three other digits (for grasping motions). Examples of glove-based devices include [28] which supports simultaneous grasping motions and [29] which supports individual movements of the fingers and thumb. A survey of robotic devices supporting the upper limb, including hand and thumb devices, can be found in Ref. [30]. A brief and focused overview of robotic devices for thumb rehabilitation are provided in Ref. [31].

All categories of hand and thumb rehabilitation devices share common challenges. What movements should be supported by the device? How many degrees-of-freedom are optimal? What sensors and actuators should be used? How will the device attach to the subject? Is the device easy to don and doff as well as adjust for different hand/thumb sizes? Each of these questions require careful consideration, and tradeoffs may have to be made. Assisting the thumb during grasping is particularly challenging due to its complex anatomical structure. As an approach for overcoming these challenges, a few robotic devices use a reduced number of actuated DOFs to achieve grasping motions, limiting the number of robot-assisted motions, primarily focusing on assisting a single type of grasping motion, either flexion/extension motion of the CMC and/or the MCP joint or the abduction/adduction of the CMC joint, mimicking the opening/closing motion of the thumb. The tradeoff here is made between the complexity of the design and the actuation, and the number of grasping motions supported [8,27]. Another approach includes actuating all the joints of the thumb independently to achieve all possible grasping motions, increasing the complexity of the design and requiring more precise control schemes [25,32]. Robotic devices are also sometimes limited in the capability of assisting the thumb bidirectionally, either actuating flexion or extension but not both (or either assisting only in abduction or abduction but not both) [33]. Most robotic devices are actuated with electric motors while a few are pneumatically driven [34,35]. The use of geared motors increases friction and puts the thumb at a mechanical disadvantage when interacting with the robot, while pneumatic actuation limits the actuation bandwidth. Both limit the backdrivability of the mechanism. The device in Ref. [36] is an example of a 4DOF series-elastic-actuated thumb exoskeleton capable of assisting bidirectional motions. The authors, however, indicate the device, in some cases, impedes the abduction/adduction motion of the CMC joint.

The current clinical practice for assessing thumb proprioception includes the physiotherapist moving the subject's thumb manually [37] and relying on the subject's responses in gauging the thumb's perceived location. In addition to assisting with grasping motions of the thumb, the exoskeleton presented in this work is intended to serve as a scientific tool for assessing and training thumb proprioception objectively, mitigating the ceiling/floor effects.

To our knowledge, there does not exist a thumb exoskeleton device that supports 2DOF grasping motions with therapy and assessment capabilities that can match the FINGER device. Specifically, the thumb module presented here was designed to facilitate proprioceptive assessment and training of the thumb over a broad range of thumb movement training, both requiring high-backdrivability and high-bandwidth actuation.

Design Objectives for the Thumb Individuating Grasp Exercise Robot. The parent device for this work is FINGER, a rehabilitation robot designed for finger movement therapy by moving the index and middle fingers individually through a naturalistic curling motion. Although originally designed for the administration and investigation of poststroke therapy, FINGER has a wide range of assessment and therapy capabilities. The FINGER robotic device is comprised of two lightweight and low-friction stacked 8-bar mechanisms and is driven by high-bandwidth, low-friction actuators. A few desirable attributes of the robot include, but are not limited to, high backdrivability, high controllable bandwidth, direct force control, low mechanical impedance, and adjustability to account for different hand sizes. These attributes give FINGER a broad range of capabilities for assessment (e.g., strength, proprioception, range-of-motion, etc.) and therapy (e.g., resistive, assist-as-needed, subject-initiated, etc.).

Although the thumb is a key component of grasping, the FINGER robot does not currently support assessment or movement therapy of the thumb. In addition, the design requirements of the thumb module were selected to support the investigation of the role of proprioception in poststroke movement therapy, including existing attributes of FINGER: high backdrivability, low impedance, and direct force control. The target population for use of the thumb module, in terms of functional impairment, was similar to that of the original FINGER study: chronic (six+ months) survivors of stroke with moderate to mild functional impairment defined as a minimum Box and Blocks [38] score of three blocks with 20% less blocks on the affected versus unaffected side.

The goal of the work described in this paper, therefore, was to develop an exoskeleton module to augment FINGER so that the combined robotic device could assess and assist grasping motions of the thumb simultaneously with the index and middle fingers. Although the minimum criteria specified two distinct grasping paths of the thumb, to meet the index and middle fingers individually, the resulting design also includes individual flexion–extension and abduction–adduction capabilities, enabling a wide range of thumb motions.

Design Challenges and Approach for the Thumb Individuating Grasp Exercise Robot. Creating a thumb exoskeleton module with characteristics similar to the FINGER device presented several challenges. Importantly, the motion of the thumb when grasping to meet the index and middle fingers cannot be characterized as planar; the grasping motion creates an arc and the dorsal surface of the thumb rotates, or "twists," along the trajectory from extension to flexion. Thus, a parallel and planar mechanism (e.g., 8-bar) like those utilized by FINGER could not be considered. Furthermore, recreating two independent grasping motions, to the index and middle fingers separately, requires the exoskeleton mechanism to feature 2DOFs. The solution presented

and the main contribution of this work is a spherical 5-bar mechanism that provides 2DOFs in a parallel structure employing similar actuators to the FINGER device (see Fig. 1). The optimized design recreates the curved path motion and rotation, or "twist," of the thumb during grasping to meet the index and middle fingers separately. Although not created specifically to do so, the design also facilitates independent flexion–extension and abduction– adduction of the thumb, creating a large workspace for thumb motions, which can be leveraged by future applications of the device.

The 2DOF spherical 5-bar is a five-revolute-joint (5R) parallel mechanism with all the joint axes intersecting at a common center point and the end-effector moving on the surface of the sphere. When compared to serial chain mechanisms, parallel mechanisms, in general, have lower inertial impedance due to the ability to locate the actuators at the base link; in this case, two linear actuators drive the two fixed joints of the 5-bar mechanism.

Major applications utilizing a 2DOF spherical 5-bar mechanism include device (cameras, antennas, etc.) orienting operations [39,40], minimally invasive surgical robotics [41], rehabilitation [42], and robot wrists [43]. Analysis of the kinematics (direct and inverse) can be found in Ref. [44]. Optimal design and singularity analysis as well as workspace analysis are presented in Refs. [45] and [46].

Similar to Refs. [47–49], the design approach for this mechanism involved the optimal synthesis of the structural parameters of the mechanism (link dimensions, end-effector dimensions, etc.) and configuration angles (angles for the actuated joints at each target output). In this application, a multistep mechanism synthesis process was utilized with the ultimate goal to reproduce the thumb-finger grasping trajectories. The first step used infrared motion capture cameras to quantify the trajectories (including position and rotation information) of a representative sample of subjects grasping with their thumb to meet either the index or middle fingers while connected to the FINGER robot. A sphere was then fit to the trajectories of each subject, allowing all subjects' data to be normalized to a common sphere center and radius. Next, a simple spatial serial-chain mechanism with a universal joint at the common sphere center was optimized to reproduce the index and middle finger grasping trajectories with the angles constrained to have a linear correlation. The objective of this intermediate optimization step was to obtain generalized reference trajectories (including position and rotation) of the thumb grasping to both the index and middle fingers separately for a representative sample of hands (with different thumb sizes and thumb grasping patterns). The two separate reference trajectories were sampled evenly along the curved surface of the grasp, creating 20 targets for the index finger trajectory and 20 targets for the middle finger trajectory. Notably, the target trajectories featured not only the curved path of the grasping motions but also the natural rotation "twist" of the thumb relative to the grasping direction along the path. This anatomical grasping feature was a principal challenge that was met by the characteristics of the spherical 5-bar mechanism, which was synthesized in the final step to reproduce the target trajectories.

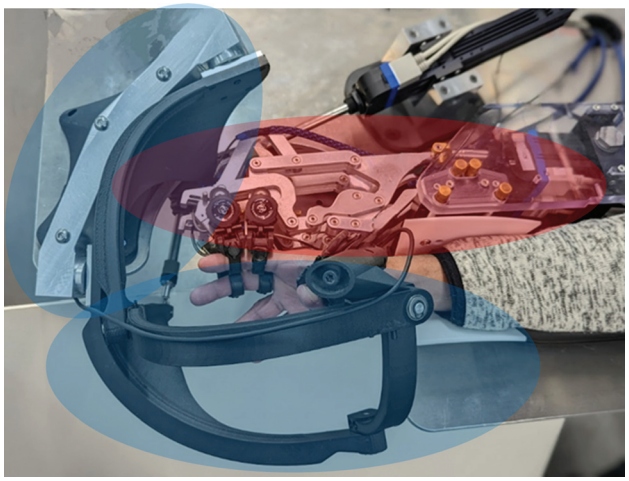

Fig. 1 The 2DOF spherical 5-bar exoskeleton thumb module, THINGER (blue), supports thumb flexion/extension and abduction/adduction. The parent device, FINGER (red), assists the index and middle fingers individually in naturalistic grasping. Together, the combined device allows broader proprioceptive training and assessment regimes.

A major advantage of the approach presented here is the ability to design an exoskeleton capable of reproducing the thumb-finger grasping trajectories without needing to align actuators with each of the anatomical joints of the thumb, which are particularly complex. Rather, the goal is to design a mechanism capable of reproducing reduced DOF thumb grasping motions. This allows the DOFs of the mechanism to be chosen to match the desired motions, rather than the complete DOFs of the thumb, and achieves complex spatial motions with optimal actuation and minimal mass.

The sections that follow describe the complete design process in more detail, including the thumb-motion data capture in section Characterization of Thumb Grasping Trajectories, the multistep optimization process for the mechanism synthesis in section Multistep Mechanism Synthesis, mechanical device design and development in section Thumb Individuating Grasp Exercise Robot Design and Development, implementation of a preliminary force controller in section Controller Design and Actuation Hardware, and preliminary testing to demonstrate fit and function in section User Testing and Evaluation.

Characterization of Thumb Grasping Trajectories

The spatial motion of the thumb during grasping presents uniquely complex challenges compared to the finger-curling grasp motion of the FINGER robot. Thumb-curling motions like cylindrical grips, recognized as a combination of the flexion–extension and abduction–adduction motions of the CMC and MCP joints of the thumb, produce a curved surface in three-dimensional space. Determining this surface becomes the start of the multistep optimization process to design the thumb module.

Motion Capture of Thumb Grasping. The first step used infrared motion-capture cameras to quantify the trajectories (position and rotation) of a representative sample of subjects grasping with their thumb to meet either the index or middle fingers while connected to the FINGER robot. Unlike the fingers, which have three phalanges, the thumb has only two, the proximal (or middle) and distal phalanges. The only way to firmly secure the robot to the thumb without interfering with the sense of touch of the thumb tip during thumb-index and thumb-middle finger grasping is by connecting the robot to the proximal phalanx. Therefore, a three-dimensional (3D)-printed cuff with a plate of four infrared (IR) markers in the shape of a rhombus was secured to the dorsal surface of the proximal phalanx of each subject's thumb to digitize the spatial trajectories (position and rotation) of the thumb during grasping (see Fig. 2).

The motion camera setup consisted of four OptiTrack Flex13 cameras operating at 100 frames per second. The cameras were placed on the top of vertical columns forming a rectangle approximately 1 m above a work surface where FINGER was located. The motion capture ground plane was placed on the workspace close to the thumb during grasping. Markers were placed on the body of FINGER and on two moving links of the index finger 8-bar mechanism to reference the captured trajectories and the position of the thumb to the location and orientation of the robot and the moving fingers. During a data capture session, the subject's index and middle fingers were placed in the passive FINGER robot, so that the captured trajectories could be referenced to the robot's location and orientation. The Optitrack proprietary motion tracking software MOTIVE was used to record the position and orientation of all the IR markers in the work environment. All

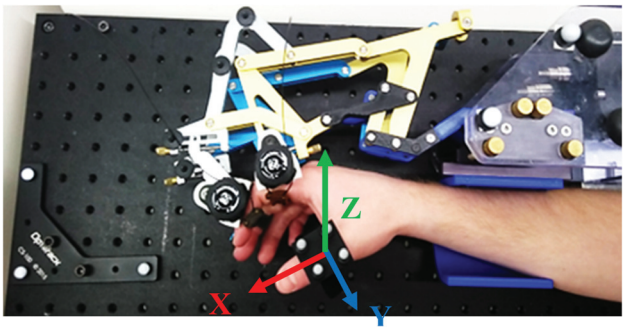

Fig. 2 Motion capture setup showing the ground plane (bottom left), IR markers in a rhombus shape located on a plate secured to the dorsal surface of the middle phalanx of thumb, IR markers on the 8-bar mechanism of the index finger, and IR markers on the base of the FINGER. The *x*-axis of the reference frame points in the flexion/extension direction, *y*-axis points in the abduction/adduction direction.

the distances and angles were measured with respect to the ground plane, and the cameras were recalibrated prior to each data capture session. The coordinate frame of the capture data was aligned such that the z-axis pointed vertically upward, the y-axis pointed away from the subject along their forearm, and the x-axis pointed to the subject's right.

Six subjects covering a wide range of hand sizes (see Table 1), having no hand movement impairment, voluntarily participated in data collection which consisted only of thumb trajectory position and rotation data. The University of Idaho's Institutional Review Board considered the data collected to be exempt from oversight since these data were only used for device development. During a data collection session, each subject was instructed to perform a natural grasp motion with their thumb from a comfortable extension position through flexing to touching either their index finger (i.e., an *index grasp*) or their middle finger (i.e., a *middle grasp*) at completion. Subjects were not given instruction regarding the shape of the grasp trajectories. They were instructed to perform the two grasp tasks (*index grasp* or *middle grasp*) alternately, repeating for 60 s at a steady and comfortable pace, followed by a period of rest. During the trials, subjects completed the finger curling aspects of the grasping while their index and middle fingers were strapped in the passive (i.e., unpowered) FINGER robot.

Thumb-Trajectory Surface Fitting and Normalization. The curved spatial surface of the thumb trajectories obtained via motion capture were found to fit the surface of a sphere with good accuracy. The accuracy of the fit was measured based on the mean distance error between the surface of the sphere and each trajectory data point (defined as the center of the rhombus plate). This was one of the key factors driving the design solution toward a spherical 5-bar mechanism.

A gradient-based solver (MATLAB's fmincon function) was used to fit a sphere to the combined trajectory data (from both *index* and *middle grasps)* of each of the six subjects. For this process, the grasp trajectories were reduced to a single point defined as the center of the four IR markers on the back of the thumb during motion capture. The cost function, J_{sphere}, for this optimization was a function of the distance between each trajectory point and the surface of the sphere

Table 1 Hand metrics of six unimpaired subjects

Hand attribute	Measurement (mm)
Hand length	178.09 ± 11.50
Palm width	84.23 ± 6.74
Thumb length	64.18 ± 2.07
Thumb circumference	63.78 ± 3.54

$$J_{\text{sphere}} = \sum_{i=1}^{n}((x_i - a)^2 + (y_i - b)^2 + (z_i - c)^2 - r^2) \quad (1)$$

where (x_i, y_i, z_i) is the ith trajectory point, (a,b,c) is the center of the sphere, r is the sphere radius, and n is the number of samples. Spheres were fit to the data of each individual subject with a mean-distance error for each data point (averaged over all the subjects) of 0.98 mm between the trajectories and the surface of the sphere. The mean sphere radius for the six subjects was 59.80 mm and the mean distance between sphere centers was 12.67 mm. These values were used to normalize all six subjects' data to a common sphere center and radius (see Fig. 3). The sphere center was located at the coordinates (51.0, −443.1, 93.3) mm with respect to the origin fixed to FINGER (see Fig. 3).

Multistep Mechanism Synthesis

The primary goals of the mechanism synthesis process were (1) to determine the kinematic design parameters of a 2DOF 5-bar mechanism capable of reproducing the thumb grasping trajectories obtained via motion capture and (2) to define best-fit smooth trajectories for both the *index grasp* and *middle grasp* tasks. Initial attempts to synthesize the 5-bar mechanism directly from the full grasp trajectory dataset were unsuccessful, primarily due to the excessive number of synthesis targets (defined as the four motion-capture points forming a rhombus plate) and the complexity of the 5-bar mechanism. Furthermore, the number of targets and the size of the solution space resulted in significant computational expense that limited the rate at which potential solutions could be found. Of the solutions that the solver did find, none of them tracked the targets with enough accuracy to constitute a viable solution. To address these problems, an intermediate synthesis step was added, which replaced the 5-bar mechanism with a kinematically simpler 2 R serial chain in which both revolute axes pass through the center of the sphere (creating a universal joint). The 2 R serial-chain synthesis was successful, producing smooth trajectory equations for both the *index grasp* and *middle grasp*. These trajectories were then spatially sampled as targets (defined again as the four rhombus-plate points) for the spherical 5-bar mechanism synthesis. Details of this multistep mechanism synthesis are given in the sections 2R Serial-Chain Synthesis and Trajectory Identification and Two Degree-of-Freedom Spherical 5-Bar Mechanism Synthesis.

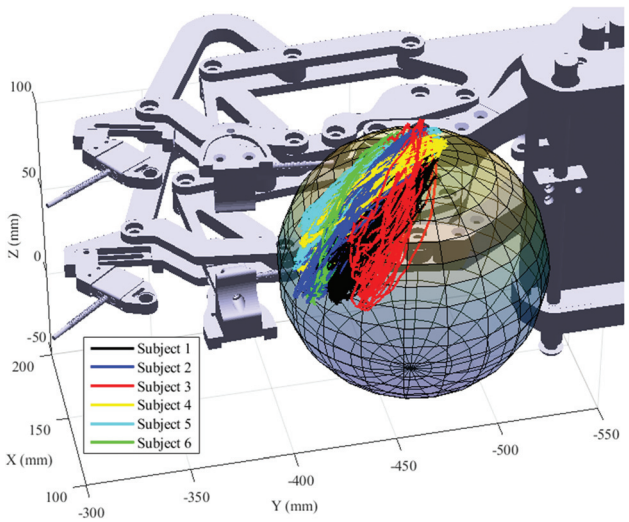

Fig. 3 Isometric view (see Fig. 1 for orientation reference) of subject trajectory data and fit sphere, after normalization to a common center and radius, shown aligned to FINGER. Six colors here represent normalized thumb grasp trajectories of the six subjects.

2R Serial-Chain Synthesis and Trajectory Identification. Figure 4 shows normalized grasp trajectories of all six subjects separated by type of grasp (red for *index grasp* and blue for *middle grasp*). The right side of Fig. 4 shows sampled rhombus-plates from motion capture (not all plates were shown for clarity). This visualization of the data highlights the large variance in grasp shape. All of the rhombus plates were used as targets for the 2 R serial-chain mechanism synthesis. The goal of the mechanism synthesis is to find the structural variables and n joint angles of the 2 R serial-chain robot that most closely reach the N motion-capture rhombus plates.

The forward kinematics of a 2 R robot, $g_{st}^{2R}(\theta)$, using the product of exponentials formula [50] can be written

$$g_{st}^{2R}(\theta_A, \theta_B) = e^{\hat{\xi}_A \theta_A} e^{\hat{\xi}_B \theta_B} g_{st}^{2R}(0) \tag{2}$$

where $g_{st}^{2R}(0) \in \mathbb{R}^{4x4}$ is the translation and rotation of the tool (end-effector) frame of the robot in the home position, θ_A and θ_B are the joint angles, and $\xi_A = [-\omega_A \times q_A \quad \omega_A]^T$ is a twist describing rotation about axis ω_A that intersects with point q_A (with a similar definition for $\xi_B = [-\omega_B \times q_B \quad \omega_B]^T$).

In the tool frame, the four motion-capture markers have the coordinates (in mm)

$$p_{1t} = \begin{bmatrix} 10.8 \\ -10 \\ 0 \end{bmatrix}, \; p_{2t} = \begin{bmatrix} 8.8 \\ 9 \\ 0 \end{bmatrix}, \; p_{3t} = \begin{bmatrix} -10.8 \\ -10 \\ 0 \end{bmatrix}, \; p_{4t} = \begin{bmatrix} -8.8 \\ -9 \\ 0 \end{bmatrix} \tag{3}$$

These four points form a rhombus centered at the tool-frame origin and match the geometry from the motion-capture thumb cuff. For a given nth configuration of the 2 R mechanism, defined by joint angles $\theta_{A,n}$ and $\theta_{B,n}$, the spatial location of the four points in Eq. (3) can be found according to

$$p_{is}^n = g_{st}^{2R}(\theta_{A,n}, \theta_{B,n}) p_{it}^n \tag{4}$$

where n indicates the nth configuration of the mechanism corresponding to each of N target rhombus plates and p_{is}^n is the spatial location of the ith rhombus point in Eq. (3), mapped from its corresponding tool frame coordinates p_{it}^n. The spatial location of these end-effector points is compared to the location of the points on the nth motion-captured rhombus plate and the squared-error is accumulated for all of the N rhombus plate targets creating the cost function

$$J_{2R} = \sum_{n=1}^{N} \sum_{i=1}^{4} (r_{is}^n - p_{is}^n)^2 \tag{5}$$

where r_{is}^n is the location of the ith point on the nth target rhombus plate.

MATLAB's fmincon function was used to minimize the cost function in Eq. (5) by changing the structural parameters (e.g., home position $g_{st}^{2R}(0)$) and the joint angles (each target rhombus plate requires different values of θ_A and θ_B). Several constraints were included in the optimization. First, the rotation axes were constrained so that $\omega_A = [0 \quad 0 \quad 1]^T$ and $\omega_A \perp \omega_B$. These constraints reduced the solution space and arranged the two revolute joints to form a universal joint at the center of the sphere. Furthermore, the rotation axes were constrained to pass through the center of the normalized sphere (moved to the origin for synthesis, so that $q_A = q_B = [0 \quad 0 \quad 0]^T$.) This constraint also reduced the solution space and ensured that the resulting solution trajectories would be reachable by the spherical 5-bar mechanism (see Fig. 5). Importantly, the angles of the joints were linearly constrained for both the *index grasp* and *middle grasp* trajectories, so that

$$\begin{aligned} \theta_A &= m_{\text{index}} \theta_B + b_{\text{index}} \\ \theta_A &= m_{\text{middle}} \theta_B + b_{\text{middle}} \end{aligned} \tag{6}$$

where m_{index}, m_{middle}, b_{index}, and b_{middle} are constant coefficients defining a linear relationship between θ_A and θ_B. This constraint

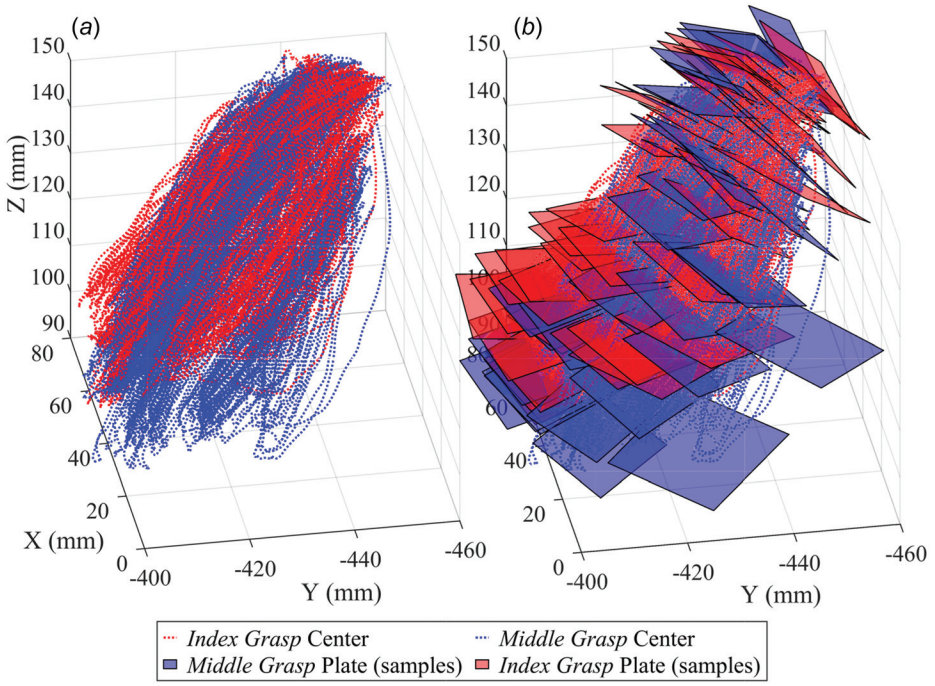

Fig. 4 (*a*) Isometric view (similar to Figs. 1 and 2) of the centers of all *index grasp* (red) and *middle grasp* (blue) trajectories. (*b*) Sampled (to declutter) motion-captured rhombus plates from *index grasp* (red) data and *middle grasp* (blue) data. The rhombus plates (all captured, not just the samples shown) were used as the targets for the 2 R serial chain mechanism synthesis.

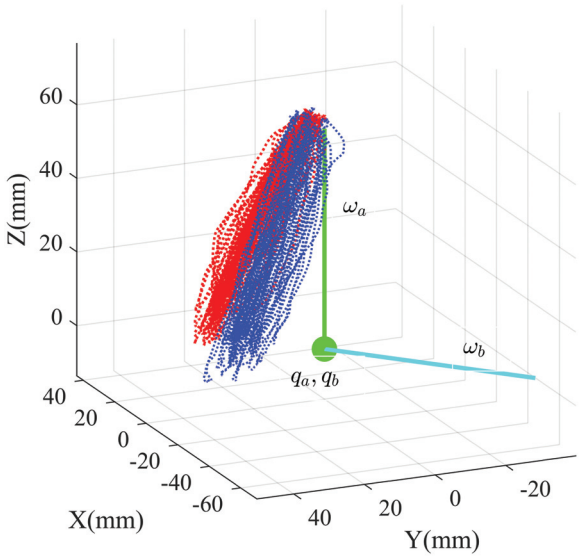

Fig. 5 Isometric view of the spatial locations of the optimized and mutually perpendicular axes of the 2 R serial-chain mechanism which reproduce the grasping motion. The axes are indicated by ω_A (green) and ω_B (cyan), with q_A and q_B located at the center of the sphere ([0,0,0]). Sampled centers of the motion-captured *index grasp* (red) and *middle grasp* (blue) trajectories are also shown for spatial reference.

forced the solver to find smooth paths for both the *index grasp* and *middle grasp* trajectories. After the constraints, the solver had 13 structural parameters, four trajectory coefficients, and 14,000 angles to determine during optimization, as summarized in Table 2.

The most important results of optimization of the 2 R serial-chain mechanism are the solutions, defined by Eq. (6), for both *index grasp* and *middle grasp* trajectories, which were each sampled at 20 spatially distributed locations (for a total of 40 rhombus-plates). Analysis of the thumb path data revealed that the subjects spent relatively more time in configurations corresponding to the extents of the thumb grasp, i.e., flexed and extended positions. Time-based sampling of the solution trajectories mistakenly skewed the optimization toward these positions. Thus, spatially sampled solutions were used as targets for the synthesis of a 2DOF spherical 5-bar mechanism as described later (targets shown in Fig. 8).

Two Degree-of-Freedom Spherical 5-Bar Mechanism Synthesis. The 2DOF spherical 5-bar mechanism consists of five revolute joints whose axes all intersect at a common center. The axes and angles of rotation of joints one through five are denoted, respectively, by $\omega_{1\text{-}5}$ and $\theta_{1\text{-}5}$. As shown in Fig. 6, axes ω_1 and ω_5 are fixed to a ground link and are actuated. The other four links connect the remaining links in succession: Link12, Link23, Link34, and Link45.

The forward kinematics of a parallel mechanism can be expressed by equating multiple serial chains to form a structure or

Table 2 2 R serial-chain mechanism synthesis parameters

Parameter description	No. of parameters
Home position $g_{st}^{2R}(0)$ translation	3
Home position $g_{st}^{2R}(0)$ rotation axis and angle	4
Joint axes ω_A and ω_B	6
Index grasp trajectory coefficients m_{index} and b_{index}	2
Middle grasp trajectory coefficients m_{middle} and b_{index}	2
Joint angle $\theta_{B,n}$ for each target plate n	14,000

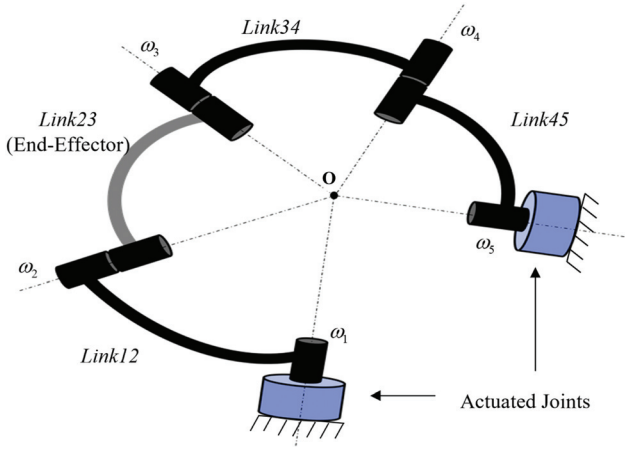

Fig. 6 A 2DOF spherical 5-bar mechanism with all five axes intersecting at a common center. Rotation axes ω_1 and ω_5 are the fixed and actuated joints.

loop equation [41,46]. In this case, the spherical 5-bar can be described with two serial chains: (1) a left chain comprised of axes $\omega_{1\text{-}2}$ and (2) a right chain comprised of axes $\omega_{3\text{-}5}$. The resulting forward kinematic equations are

$$g_{st}^{12}(\theta) = e^{\hat{\xi}_1\theta_1}e^{\hat{\xi}_2\theta_2}g_{st}(0)$$
$$g_{st}^{543}(\theta) = e^{\hat{\xi}_5\theta_5}e^{\hat{\xi}_4\theta_4}e^{\hat{\xi}_3\theta_3}g_{st}(0) \tag{7}$$

where $g_{st}(0) \in \mathbb{R}^{4\times4}$ is the home position of the tool (end-effector) frame located on Link23, $\theta_{1\text{-}5}$ are the joint angles, and $\xi_i = [-\omega_i \times q_i \quad \omega_i]^T$ is a twist describing rotation about axis ω_i that intersects with point q_i, defined for joints 1-5. Following the 2 R serial-chain synthesis, the four motion-capture markers have the tool frame coordinates defined in Eq. (3). For a given nth configuration of the 5-bar mechanism, defined by joint angles $\theta_{1,n}$ and $\theta_{2,n}$, the spatial location of the four points in Eq. (3) can be found according to

$$p_{is}^n = g_{st}^{12}(\theta_1,\theta_2)p_{it}^n$$
$$p_{is}^n = g_{st}^{543}(\theta_5,\theta_4,\theta_3)p_{it}^n \tag{8}$$

where n indicates the nth configuration of the mechanism corresponding to each of $N = 40$ target rhombus plates and p_{is}^n is the

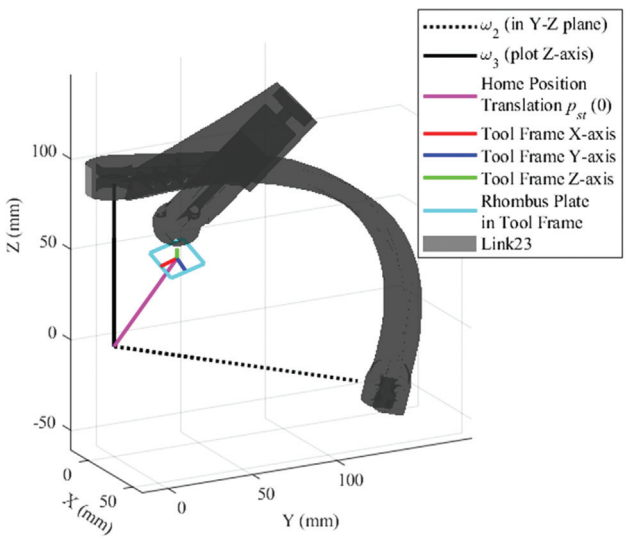

Fig. 7 Tool frame location in the home position. The tool frame is rigidly attached to Link23, connecting axis ω_2 and axis ω_3.

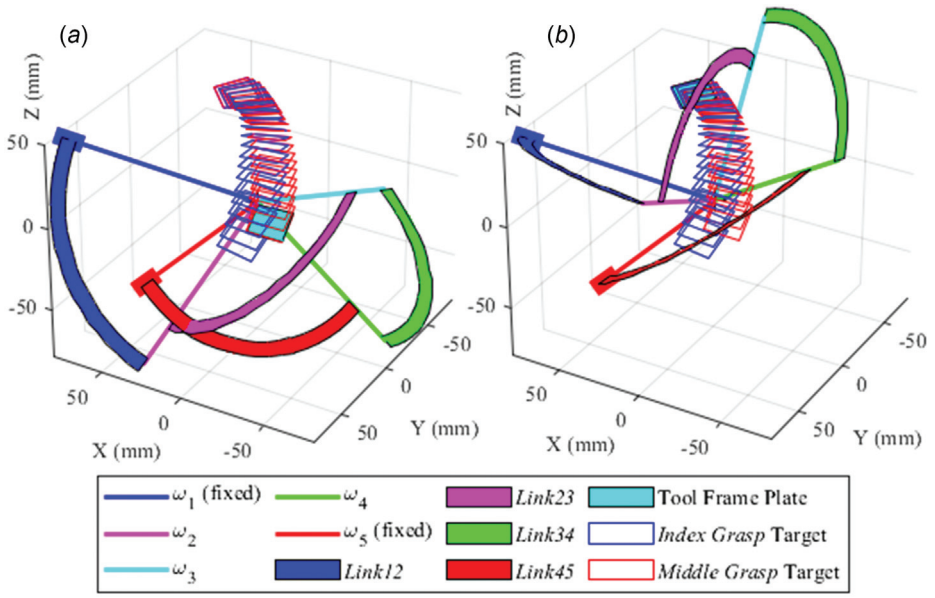

Fig. 8 (*a*) 5-bar mechanism in the flexed (grasped) configuration. (*b*) 5-bar mechanism in the fully extended configuration. In both visualizations, tool frame output is shown as cyan rhombus plate. The end-effector, fixed to Link23, recreates the grasp trajectories, passing through the target rhombus plates (blue and red). Both visualizations are from viewpoints similar to previous figures.

spatial location of the *i*th rhombus point in Eq. (3), mapped from its corresponding tool frame coordinates p_{it}^n. Either of the two equations in Eq. (8) could be used to find the spatial locations of the four points, as both the equations represent the forward kinematics of mechanism (the first equation uses the left serial chain while the second equation uses the right serial chain). The spatial location of these end-effector points are compared to the location of the points on the *n*th motion-captured rhombus plate and the squared-error is accumulated for all of the *N* rhombus plate targets creating the cost function

$$J_{5\text{bar}} = \sum_{n=1}^{N=40} \sum_{i=1}^{4} (r_{is}^n - p_{is}^n)^2 \tag{9}$$

where r_{is}^n is the location of the *i*th point on the *n*th target rhombus plate.

As for the 2 R serial-chain synthesis, a gradient-based solver (MATLAB's fmincon function) was used to minimize the cost function in Eq. (9) by changing the structural parameters and the joint angles. Multiple constraints and penalties were included in the optimization. A symmetric solution was desired for ease of calculation of the inverse kinematics, so the angle of Link12 was constrained to equal the angle of Link45 ($\angle\omega_1\omega_2 = \angle\omega_4\omega_5$) and the angle of Link23 was constrained to equal the angle of Link34 ($\angle\omega_2\omega_3 = \angle\omega_3\omega_4$). The angle between fixed axes ω_1 and ω_5 was constrained to 60 deg, placed initially at $\omega_1 = \begin{bmatrix} -\frac{1}{2} & -\frac{\sqrt{3}}{2} & 0 \end{bmatrix}^T$ and $\omega_5 = \begin{bmatrix} \frac{1}{2} & -\frac{\sqrt{3}}{2} & 0 \end{bmatrix}^T$ before both were rotated first −30 deg about the *y*-axis and then −45 deg about the *z*-axis. These locations were chosen to align the most manipulable direction of the mechanism with the largest movement direction of the motion (as seen in Fig. 6). The manipulability of the mechanism at each configuration was measured by analyzing the inverse condition number of the body manipulator Jacobian, which was obtained by calculating the ratio of the minimum and the maximum singular value of the body manipulator Jacobian [50]. A penalty term was added to the cost function that calculated manipulability at every output configuration of the mechanism. After the constraints, the solver had 16 structural parameters and 200 angles to determine during optimization, as summarized in Table 3.

After many minimizations of the cost-function starting from randomized initial conditions, a feasible symmetrical solution was found. The mean distance error for each point (four per rhombus), averaged over the 40 target locations was 0.402 mm. For the structural parameters, the solution produced the home configuration of the tool frame (see Fig. 7) and the moving rotation axes

$$g_{st}(0) = \begin{bmatrix} 0.4966 & 0.8448 & -0.1993 & -37.6107 \\ -0.7319 & 0.2840 & -0.6194 & 4.9629 \\ -0.4667 & 0.4535 & 0.7593 & 45.7118 \\ 0 & 0 & 0 & 1 \end{bmatrix}$$

$$\omega_2 = \begin{bmatrix} -0.0655 \\ 0.9888 \\ 0.1338 \end{bmatrix}, \omega_3 = \begin{bmatrix} -0.7849 \\ -0.3957 \\ 0.4768 \end{bmatrix}, \omega_4 = \begin{bmatrix} -0.6013 \\ -0.2171 \\ -0.7689 \end{bmatrix} \tag{10}$$

This solution found $\angle\omega_1\omega_2$ and $\angle\omega_4\omega_5$ to be close to 106.02 deg and $\angle\omega_2\omega_3$ and $\angle\omega_3\omega_4$ to be close to 101.03 deg. A visualization of the solution is shown in Fig. 8, including a flexed (grasped) pose in Fig. 8(*a*) and a fully extended (thumbs up) pose in Fig. 8(*b*).

The optimization also finds 40 solution angles for each of $\theta_{1\text{-}5}$. Figure 9(*a*) shows the joint angles for both the *index grasp* and *middle grasp* trajectories. All the joint angles have smooth curves indicating that the mechanism maintains its structure while avoiding a singular configuration. These angles are common in full extension, so that the thumb extension position is shared for both

Table 3 5-bar spherical mechanism synthesis parameters

Parameter description	No. of parameters
Home position $g_{st}(0)$ translation	3
Home position $g_{st}(0)$ rotation axis and angle	4
Joint axes ω_3, ω_4, and ω_5	9
Joint angles $\theta_{1,n}$, $\theta_{2,n}$, $\theta_{3,n}$, $\theta_{4,n}$, and $\theta_{5,n}$ for target plate n	$4 \times 5 = 200$

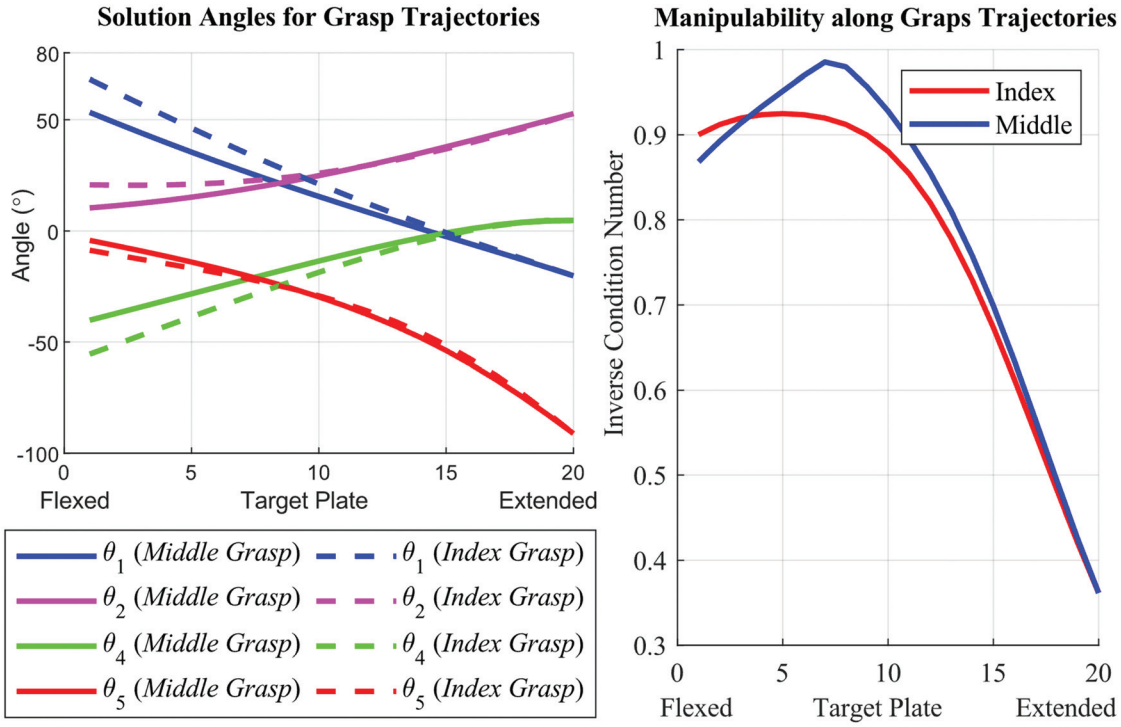

Fig. 9 (*a*) Joint angles of the optimized 5-bar mechanism transitioning from flexed (grasped) to extended. Trajectories for the *index grasp* are shown as dashed curves and *middle grasp* are shown as solid curves. The trajectories share common angles at thumb extension. (*b*) Manipulability of the 5-bar mechanism as it moves from the flexed to the extended configuration for both the trajectories. (*a*) Solution angles for grasp trajectories and (*b*) manipulability along grasp trajectories.

grasps. During grasping, the mechanism avoids singularities and maintains good manipulability, greater than 0.3 across both the grasping motions. Figure 9(*b*) shows the manipulability of the configuration for each of the 40 poses.

Thumb Individuating Grasp Exercise Robot Design and Development

This section details the mechanical design and development of the 2DOF spherical 5-bar thumb exoskeleton. The design is based on the kinematic parameters obtained from the mechanism synthesis described in the section Multistep Mechanism Synthesis.

Thumb Exoskeleton Mechanical Design. The mechanical location of these joint axes ω_1 and ω_5 were placed behind the hand at a large enough distance from the sphere center to avoid interference with FINGER during operation (see Fig. 10). This location minimizes the visual obstruction to the user's view of the hand as opposed to placing the joints on the opposite side of the sphere directly between the user and their hand. Another advantage of this location is that the two linear Servotube actuators (Dunkermotoren), can be placed safely away from the user. An aluminum base link provides accurate alignment between fixed axes ω_1 and ω_5 and provides housing for their respective bearings. A 3D-printed riser positions this base link at the correct coordinates and angles above the base plate on which FINGER is secured.

The locations of the remaining three axes are not fixed and move as the mechanism is actuated. The design of the links that connect all five axes is governed by the optimized solution from mechanism synthesis: Link12 ($\angle\omega_1\omega_2$) and Link45 ($\angle\omega_4\omega_5$) must form a 106.026 deg angle; Link23 ($\angle\omega_2\omega_3$) and Link34 ($\angle\omega_3\omega_4$) must form a 101.029 deg angle. These links were designed to avoid contact not only with each other during actuation but also with the user's hand and the FINGER device. Axis shafts for all joints were machined from high-strength aluminum, and two deep-groove ball bearings allowed low-friction motion of each joint. The four moving curved links were 3D printed with carbon-fiber reinforcement layers using the Markedforged Mark Two™, resulting in a sufficiently strong and stiff mechanism.

Thumb Cuff Design and Hand Size Adjustment. The 3D thumb cuff extends out from the output Link23 (Fig. 11), securing the user to the mechanism. The user's thumb is secured using a BOA® dial, which guides the cable around a tear drop-shaped notch on the 3D-printed strap (Figs. 11(*a*) and 11(*b*)). The BOA® cable and dial simplifies the process of donning and doffing, and the 3D-printed strap with added foam padding creates a secure connection while minimizing discomfort and abrasions. An oval-shaped sliding mechanism connects the thumb cuff to Link23 (see Figs. 11(*c*) and 11(*d*)). The slider can be extended and retracted to accommodate different hand sizes, moving the user's thumb toward and away from the trajectory sphere center, essentially changing the radius of the grasp trajectory sphere. Once the thumb is secured firmly using foam padding and elastic finger sleeves to prevent skin irritation, the thumb cuff still allows smaller misalignments of the thumb within the cuff for comfort without affecting the device's capability in assisting flexion/extension and abduction/adduction motion. The specific accuracy of the device in tracking the desired grasping motion is not as important as allowing the flexion/extension and abduction/adduction motion of the thumb.

Controller Design and Actuation Hardware

A preliminary low-level force controller was implemented to reduce the impedance of the mechanism to subject-initiated motion during initial testing and evaluation (Fig. 12). The force controller uses experimentally determined models for gravity and friction compensation, and a proportional-derivative controller responds to subject forces as measured by an ATI Nano25 force/torque (F/T) transducer. Data acquisition and control is implemented on the Speedgoat® real-time target computer with

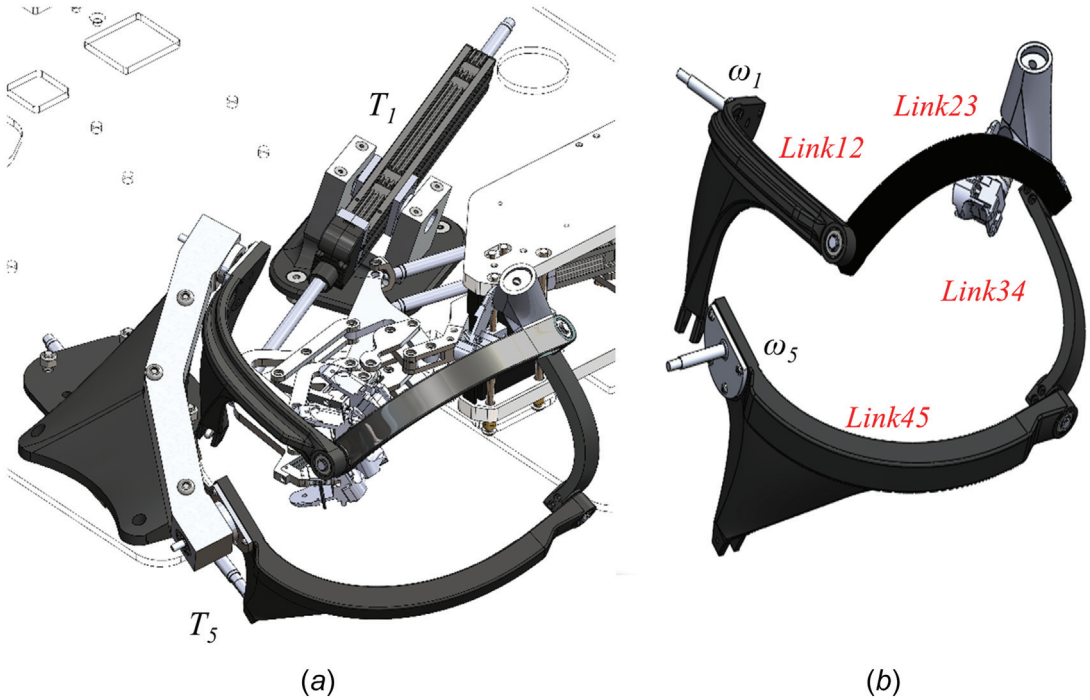

Fig. 10 (*a*) SOLIDWORKS assembly showing the spherical 5-bar thumb exoskeleton aligned with FINGER. The fixed joint ω_1 is driven by linear actuator T_1 located on top of the baseplate (shown as wireframe for clarity); ω_5 is driven by T_5 located on the underside of the base plate. (*b*) Isolated view of the spherical 5-bar mechanism.

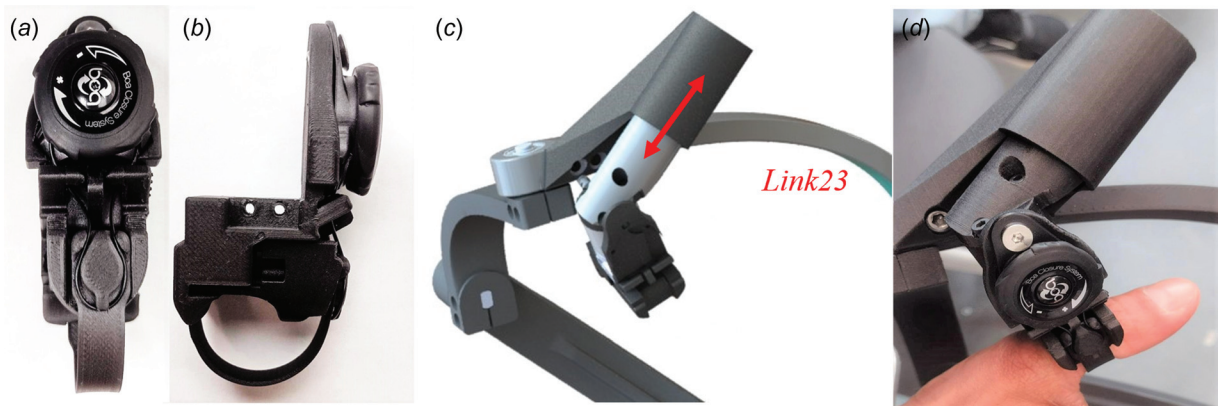

Fig. 11 (*a*) and (*b*) BOA dial and the 3D-printed strap adjustable cuff allows the thumb to be fastened securely to the thumb. (*c*) Thumb cuff and adjustment slider shown secured to Link23, arrow (red) indicates the direction of slider movement to accommodate different hand sizes. (*d*) Slider shown in extended and retracted positions. The offset slider axis moves the center of the user's thumb toward and away from the center of the sphere thumb trajectory sphere.

Simulink Real-Time from MathWorks®. An EtherCAT network acquires signals from the F/T transducer and sends commands to a Copley Accelnet Plus dual axis motor driver, which controls the two brushless linear Servotube motors (Dunkermotoren STA1116 and STA1104) that actuate the thumb exoskeleton.

The robot is integrated with the interactive RehabHero game (an interactive game similar to GuitarHero®), intended to assist subjects during therapy and assessment. The desired trajectories generated by the trajectory calculator block are linked to the interactive computer game environment. Other therapy games and assessments are under development that will incorporate the wider range of thumb motions supported by the 5-bar mechanism.

User Testing and Evaluation

The functionality of the spherical 5-bar thumb exoskeleton was tested on both impaired and unimpaired subjects. The participants provided informed consent as per the protocol approved by the Institutional Review Board at UC Irvine. The study is registered on[2] (NCT04818073). Multiple aspects were evaluated, including donning, doffing, and comfort. Figure 13 shows a healthy subject using the 5-bar thumb exoskeleton with the FINGER device. The workspace of the thumb in the exoskeleton was also evaluated, both along the *index grasp* and *middle grasp* trajectories (Fig. 14), and in exploratory directions combining flexion/extension and abduction/adduction to determine the extent of the functional workspace of the device (Fig. 15). Table 4 compares the average forces felt by the user with and without the gravity compensation, friction compensation, and force feedback. A mirrored version of the mechanism was also assembled, supporting subjects with either left- or right-side impairment.

[2]Clinicaltrials.gov

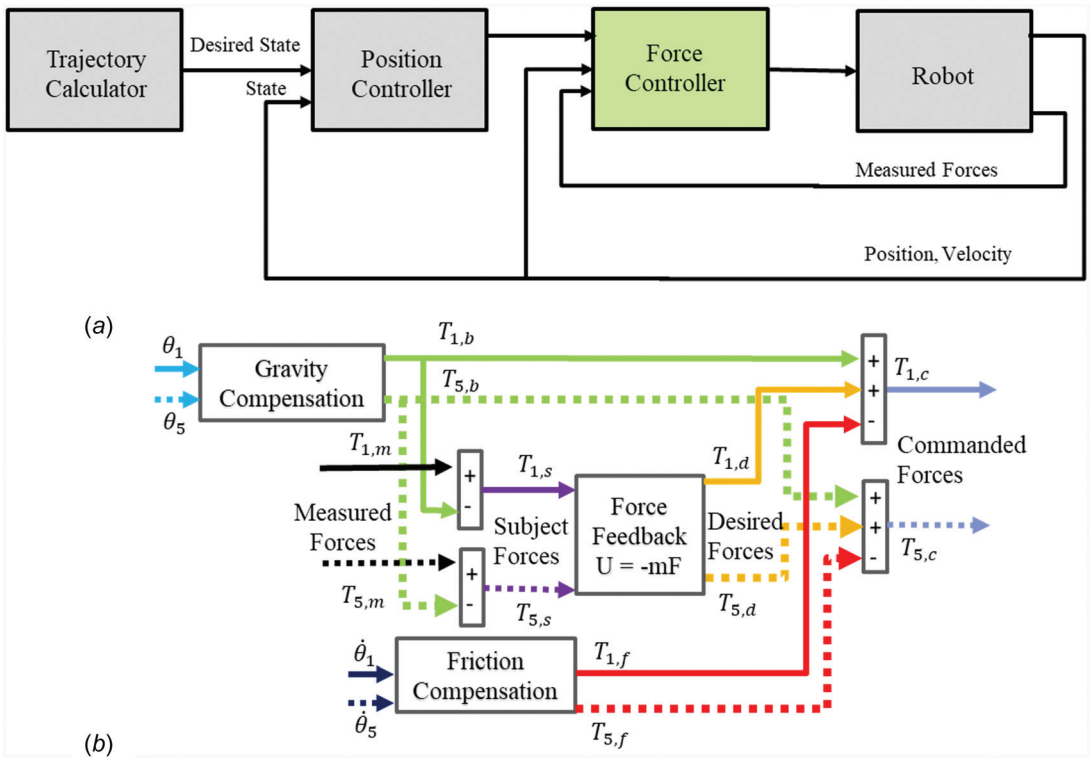

Fig. 12 (*a*) Block diagram of the implemented control system. (*b*) Force control diagram, including gravity and friction compensators for the two thumb mechanism actuators T_1 and T_5.

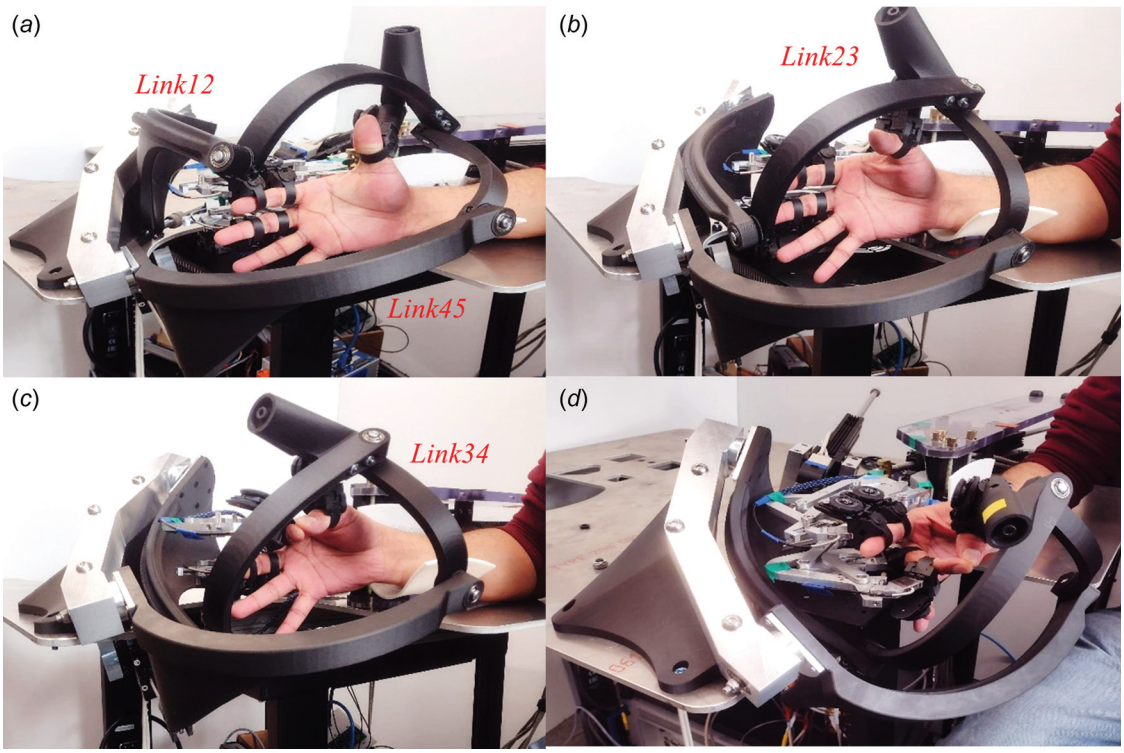

Fig. 13 A subject's hand using the FINGER device with the 5-bar spherical thumb exoskeleton module. (*a*) Thumb in the extended position. (*b*) Thumb during partial grasps. (*c*) Completion of the *index grasp*, where the thumb grasps to meet the index finger. (*d*) Completion of the *middle grasp* where the thumb grasps to meet the middle finger.

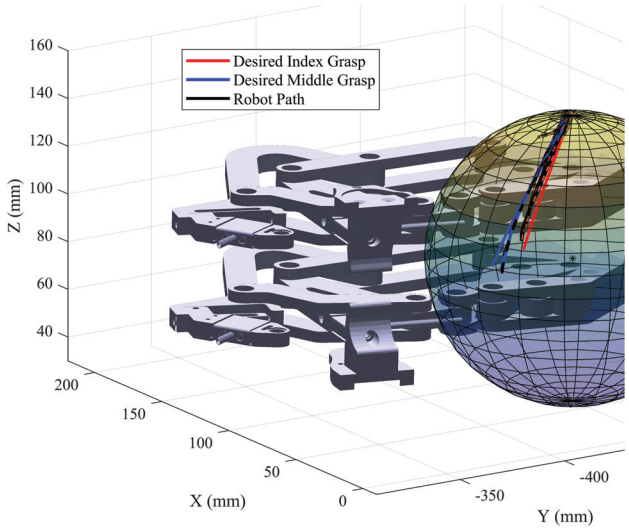

Fig. 14 Desired and robot-guided trajectories along the optimized thumb *index grasp* and *middle grasp*. The flexion/extension and abduction/adduction direction are tangential to the surface of the sphere with the flexion/extension direction aligned tangential to the desired trajectories shown.

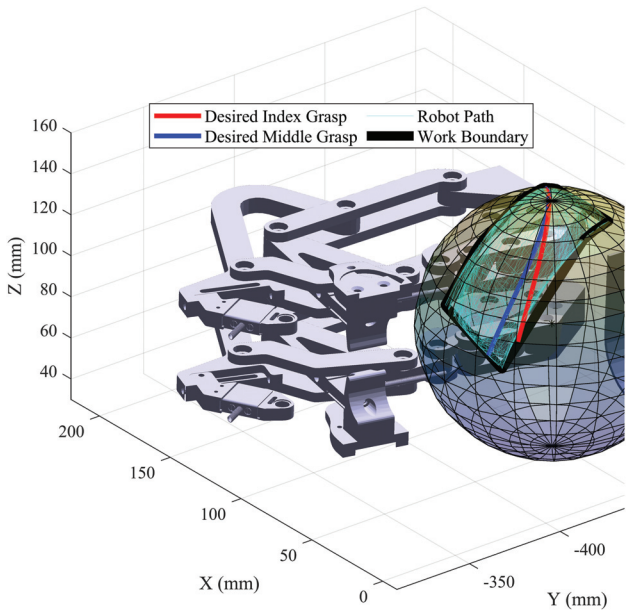

Fig. 15 Workspace of the thumb under free motion. Subject-driven motions (cyan) were recorded with the thumb attached to the robot with the intention of identifying the workspace boundaries (black). The *index grasp* (red) and the *middle grasp* (blue) trajectories are also shown here for visual comparison.

Table 4 Comparison of average forces along the 2DOFs with and without compensation

Motion direction	Flexion/extension		Abduction/adduction	
Compensation	No	Yes	No	Yes
Average force experienced	4.99 N	3.99 N	4.19 N	3.04 N
Gravity compensator forces	—	0.47 N	—	1.35 N
Friction compensator forces	—	0.33 N	—	0.22 N
Force-feedback	—	1.36 N	—	0.29 N
Peak force	15.31 N	11.03 N	16.68 N	10.38 N

We evaluated the feasibility of the thumb mechanism in four poststroke individuals in a 1.5-h training session. The subjects' ages ranged from 42 to 74 with a mean age of 62, with a box and blocks score of 23.5 (16–28). During the training session, the thumb was held in a constant thumbs up position (Fig. 16(*a*)) or moved passively between a thumbs up position to a position with the thumb in opposition to the middle finger (Fig. 16(*d*)), passing through the intermediate postures shown in Fig. 16. While the thumb was controlled passively, participants made volitional flexion/extension movements of their index and middle fingers to play computer-based games. To prevent any skin irritation in the device, participants wore elastic finger sleeves. Three of these individuals completed a single session in the device, while the fourth individual completed 12 sessions. Across all sessions, there were no recorded instances of skin abrasion nor pain during task execution when queried. Following each session, all participants reported zero pain with and without movement of the hand assessed via the visual analogue pain scale.

Discussion and Conclusions

The presented design approach was successful in producing a 2DOF spherical 5-bar exoskeleton, named thumb individuating grasp exercise robot (THINGER), capable of guiding the thumb through multiple grasping patterns. During grasping, the mechanism avoids singularities and maintains an inverse condition number (measure of manipulability) of greater than 0.3. The mechanism not only assists in guiding the thumb along the *index grasp* and *middle grasp* motions but also allows for more general thumb motion combinations of flex–extension and abduction–adduction. This versatility supports different orientations of the thumb and enables a broader range of motions for movement therapy and assessment.

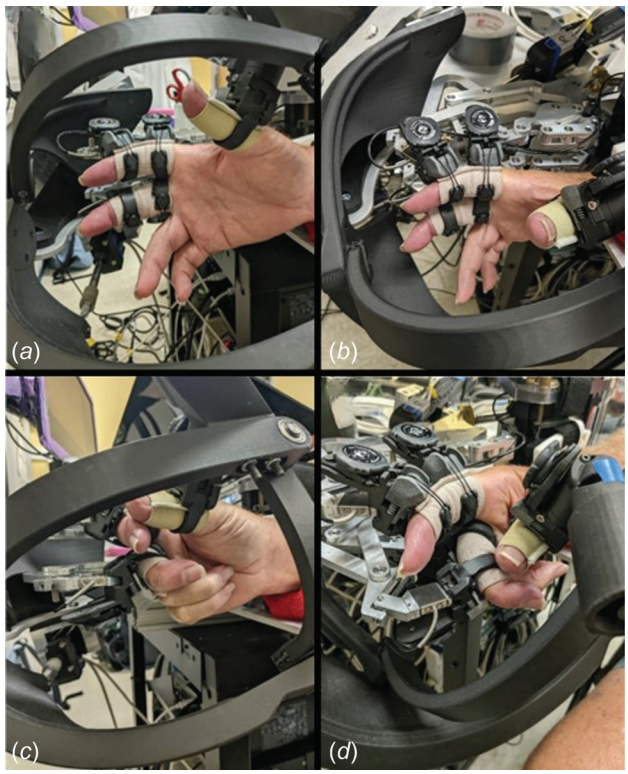

Fig. 16 A poststroke individual's hand using the FINGER device with the spherical 5-bar thumb exoskeleton module (THINGER). (*a*) Thumb in the extended position. (*b*) Thumb partially flexed along grasp path. (*c*) Completion of the *index grasp* where the thumb grasps to meet the index finger. (*d*) Completion of the *middle grasp* where the thumb grasps to meet the middle finger.

Thumb individuating grasp exercise robot works in tandem with FINGER to facilitate multidigit, individual grasping of the thumb and both index and middle fingers. A custom, adjustable thumb cuff secures the subject to the exoskeleton while an adjustable slider can move the center of the subject's thumb along the adjustment axis to accommodate a wide range of hand sizes. A preliminary force controller was implemented to reduce the resistive forces experienced by the subject during initial evaluation. The force controller includes gravity and friction compensation and utilized F/T measurements in the feedback controller to minimize interaction forces between the robot and the subject during subject-initiated movements. Future work includes: (1) implementing an impedance controller to further reduce the apparent mass of the robot and facilitate a broader set of therapy and assessment paradigms and (2) developing additional game-based interactive environments for assessment and therapy of human subjects.

Design Approach Advantages for Medical and Other Human-Robot Devices. In simplified terms, the presented design approach can be described as synthesizing a mechanism to reproduce desired motions or a specified workspace. These motions may represent a subset of the full capabilities of the targeted limb(s). In many applications involving human subjects, such as hand grasping [20], arm reaching, and walking [51], this results in a mechanism with acceptable and advantageous tradeoffs.

Parallel mechanisms can map N actuated degrees-of-freedom to Nth order surfaces. In the work presented here, the spherical 5-bar parallel mechanism maps $N = 2$ linear actuators to a two-dimensional spherical surface with an output link that also properly applies a naturalistic rotation "twist" to the thumb during thumb grasping. Another example is FINGER (which THINGER augments), which utilizes planar 8-bar mechanisms to map linear actuators to naturalistic curved planar motions with outputs at both the proximal and middle phalanges that also provide proper rotation during finger grasping. In short, using parallel mechanisms allows the designer to select the minimum degrees-of-freedom necessary by utilizing those N degrees-of-freedom along complex Nth dimensional surfaces.

This approach is an alternative to traditional exoskeleton design which typically aims to align mechanical joints with anatomical joints of the targeted limb or digit. Removing this joint alignment requirement is a significant advantage for medical and other robotic devices intended to assist human motion (i.e., exoskeletons) and/or interact with the human anatomy (e.g., surgical robots). This has several other advantages, including reduced actuation, reduced joint complexity, and more options in placement of actuators. The approach may also be applied to more complicated limbs and motions or to completely different fields altogether. The main drawback is optimization complexity, which can be at least partially addressed by the intermediate optimization step approach presented here.

Addressing Synthesis Optimization Challenges With an Intermediate Step. Synthesizing a complex parallel mechanism to reproduce spatial trajectories (consisting of positions and rotations) of targeted human motions is not without significant challenges. Human motion is inherently and notoriously noisy, both within and across subjects. Furthermore, the optimization solution space for parallel mechanisms is large for even simple mechanisms, and it increases exponentially with added degrees-of-freedom. Identifying an Nth order surface and a simplified mechanism (typically serial chain) as an intermediate optimization step can transform an insurmountable optimization problem to one with an attainable solution space that can be fine-tuned for the specifics of the application via optimization constraints and penalties. In the case of the thumb, we were unable to synthesize the 5-bar mechanism from the original motion captured data. However, we found that grasping trajectories could be closely approximated as movement with rotation (also known as "twist") on the surface of a sphere. A spherical 5-bar mechanism was selected for its ability to produce such motions, and a multistep synthesis process found a kinematically feasible solution that we were not able to find by synthesizing the final design directly from the raw motion-capture data. This multistep process effectively optimized grasp trajectories as an intermediate step to greatly reduce the design space for the synthesis of the spherical 5-bar mechanism. This multistep synthesis approach may be applied to various problems and should be considered in all mechanism synthesis attempts.

Limitation of Thumb Trajectory Data Collection. A notable limitation of this work is the limited number of subjects (six) who participated in thumb trajectory motion capture. Original plans to include a significantly larger number of subjects for the characterization of thumb grasping were halted by the pandemic. However, the six participants did represent a large range of hand sizes (see Fig. 2) and shapes, and the collected trajectory data featured a high variability. The range of hand sizes was also apparent in the intermediate optimization step, which fit a sphere to each subjects' trajectory data. For the six subjects, the sphere radii ranged from 49.8 mm to 68.6 mm with a mean of 59.8 mm and a standard deviation of 6.0 mm.

It should be noted that even with the limits of the collected trajectory data, the resulting mechanism has subsequently fit numerous users with a wide range of hand sizes. The adjustable slider between the thumb cuff and the output link of the 5-bar mechanism allows 50 mm adjustment of the sphere radius, providing for a greater range of hand sizes than that of the subjects whose range of optimized sphere radii was 18.8 mm.

Limitation of Thumb Motions Facilitated by Thumb Individuating Grasp Exercise Robot. The original design criteria specified two distinct thumb-grasping motions, one to meet the index finger during grasp and the other to meet the middle finger during grasp. Subjects had their index and middle fingers in the FINGER device during thumb trajectory motion capture and were instructed to alternate between grasping to meet those fingers (their only instruction). As such, their thumb trajectories tended toward spherical grips, driven primarily by the CMC and MCP joints (see Fig. 2) with the interphalangeal joint free to move. The present spherical 5-bar mechanism used in THINGER successfully reproduces these thumb-grasping motions but also allows for broader flexion–extension and abduction–extension stemming from the CMC and MCP joints. Although not part of the original design requirements, this was a very welcome feature of the design as it allows a much broader range of motion for assessments and therapies (e.g., strength, range-of-motion, and proprioception).

Although the presented design exceeds the design criteria in several ways, it still limits thumb motions. Tripod pinch, lateral pinch, and extension grip are examples of hand grasping motions involving the thumb that are not facilitated by the 5-bar mechanism. In many applications, such a thumb movement training and assessment for survivors of stroke, this is an acceptable tradeoff as the recovery goals for survivors of stroke (and similar impairments) are typically function focused (e.g., return an impaired hand to functional grasping of doorknobs, silverware, etc.). Furthermore, the limits on thumb motion provided by THINGER are similar to the limits on finger motion provided by FINGER; both reduce grasping complexity in exchange for high backdrivability and high controllable bandwidth, enabling unique capabilities for poststroke therapy and assessment.

Acknowledgment

The authors acknowledge the computer-aided-design and fabrication work of multiple contributors: Marshall Townsend, Royal Elder, Avery Frazier, Ryan Burr, Jack Gonzalez, and Ian Glasgow.

Funding Data

- NIH-R01HD062744 from the National Center for Medical Rehabilitation Research at the National Institute of Child Health and Human Development (Funder ID: 10.13039/100006937).

Data Availability Statement

The datasets generated and supporting the findings of this article are obtainable from the corresponding author upon reasonable request.

Nomenclature

(a, b, c) = center of the fitted sphere
$g_{st}^{2R}(0)$ = the translation and rotation of the tool (end-effector) frame of the robot in the home position
$g_{st}^{2R}(\theta)$ = rotation and translation of the tool frame by angle θ, describing the forward kinematics of the 2R mechanism
$g_{st}^{12}(\theta)$ = rotation and translation of the tool frame by angle θ, describing the forward kinematics of the left serial chain of the 5-bar
$g_{st}^{543}(\theta)$ = rotation and translation of the tool frame by angle θ, describing the forward kinematics of the right serial chain of the 5-bar
J_{sphere} = cost function for fitting a sphere to the normalized data
J_{2R} = cost function for the 2R serial-chain mechanism synthesis
$J_{5\text{bar}}$ = cost function for the 5-bar mechanism synthesis
$m_{\text{index}}, b_{\text{index}}$ = *index grasp* trajectory coefficients
$m_{\text{middle}}, b_{\text{middle}}$ = *middle grasp* trajectory coefficients
n = number of samples
p_{is} = location of the ith motion-capture rhombus marker in the spatial frame
p_{it} = location of the ith motion-capture rhombus marker in the tool-frame
p_{is}^{n} = location of the ith motion-capture rhombus marker for the configuration of the 2R mechanism, in the spatial frame
p_{it}^{n} = location of the ith motion-capture rhombus marker for the nth configuration of the 2R mechanism, in the tool-frame
q = position of a point in space with respect to the tool frame
r = radius of the fitted sphere
r_{is}^{n} = location of the ith point on the nth target rhombus plate
T_1 = actuator mounted on top of the base plate which drives ω_1
T_5 = actuator mounted on top of the base plate which drives ω_5
(x_i, y_i, z_i) = spatial coordinates of the ith trajectory point
2R = two revolute joint serial-chain mechanism
θ_A, θ_B = joint angles of the 2R mechanism
$\theta_{A,n}, \theta_{B,n}$ = joint angles for a given nth configuration of the 2R mechanism
ξ_A = twist describing rotation about axis ω_A that intersects with point q_A
ξ_B = twist describing rotation about axis ω_B that intersects with point q_B
ω = axis of rotation

References

[1] Mozaffarian, D., Benjamin, E. J., Go, A. S., Arnett, D. K., Blaha, M. J., Cushman, M., Das, S. R., et al., 2016, "Executive Summary: Heart Disease and Stroke Statistics-2016 Update: A Report From the American Heart Association," Circulation, **133**(4), pp. 447–454.
[2] Dobkin, B. H., 2005, "Clinical Practice. Rehabilitation After Stroke," N. Engl. J. Med., **352**(16), pp. 1677–1684.
[3] Yue, Z., Zhang, X., and Wang, J., 2017, "Hand Rehabilitation Robotics on Post-stroke Motor Recovery," Behav. Neurol., **2017**(3908135), pp. 1–20.
[4] Benjamin, E. J., Blaha, M. J., Chiuve, S. E., Cushman, M., Das, S. R., Deo, R., de Ferranti, S. D., et al., 2017, "Heart Disease and Stroke Statistics-2017 Update: A Report From the American Heart Association," Circulation, **135**(10), pp. e146–e603.
[5] Lum, P. S., Burgar, C. G., Shor, P. C., Majmundar, M., and van der Loos, M., 2002, "Robot-Assisted Movement Training Compared With Conventional Therapy Techniques for the Rehabilitation of Upper-Limb Motor Function After Stroke," Arch. Phys. Med. Rehabil., **83**(7), pp. 952–959.
[6] Kawashimo, J., Yamanoi, Y., and Kato, R., 2017, "Development of Easily Wearable Assistive Device With Elastic Exoskeleton for Paralyzed Hand," 2017 26th IEEE International Symposium on Robot and Human Interactive Communication (RO-MAN), Lisbon, Portugal, Aug. 28–Sept. 1, pp. 1159–1164.
[7] McConnell, A., Kong, X., and Vargas, P. A., 2014, "A Novel Robotic Assistive Device for Stroke Rehabilitation," 23rd IEEE International Symposium on Robot and Human Interactive Communication, Edinburgh, UK, Aug. 25–29, pp. 917–923.
[8] Schabowsky, C. N., Godfrey, S. B., Holley, R. J., and Lum, P. S., 2010, "Development and Pilot Testing of HEXORR: Hand Exoskeleton Rehabilitation Robot," J. Neuroeng. Rehabil., **7**(1), pp. 1–16.
[9] Maclean, N., Pound, P., Wolfe, C., and Rudd, A., 2000, "Qualitative Analysis of Stroke Patients' Motivation for Rehabilitation," BMJ, **321**(7268), pp. 1051–1054.
[10] Marchal-Crespo, L., and Reinkensmeyer, D. J., 2009, "Review of Control Strategies for Robotic Movement Training After Neurologic Injury," J. Neuroeng. Rehabil., **6**(1), pp. 1–15.
[11] Fasoli, S. E., Krebs, H. I., Stein, J., Frontera, W. R., and Hogan, N., 2003, "Effects of Robotic Therapy on Motor Impairment and Recovery in Chronic Stroke," Arch. Phys. Med. Rehabil., **84**(4), pp. 477–482.
[12] Cerasa, A., Pignolo, L., Gramigna, V., Serra, S., Olivadese, G., Rocca, F., Perrotta, P., Dolce, G., Quattrone, A., and Tonin, P., 2018, "Exoskeleton-Robot Assisted Therapy in Stroke Patients: A Lesion Mapping Study," Front. Neuroinf., **12**(44), p. 44.
[13] Gandolfi, M., Formaggio, E., Geroin, C., Storti, S. F., Galazzo, I. B., Bortolami, M., Saltuari, L., Picelli, A., Waldner, A., Manganotti, P., and Smania, N., 2018, "Quantification of Upper Limb Motor Recovery and EEG Power Changes After Robot-Assisted Bilateral Arm Training in Chronic Stroke Patients: A Prospective Pilot Study," Neural Plast., **2018**, pp. 1–15.
[14] Mochizuki, G., Centen, A., Resnick, M., Lowrey, C., Dukelow, S. P., and Scott, S. H., 2019, "Movement Kinematics and Proprioception in Post-Stroke Spasticity: Assessment Using the Kinarm Robotic Exoskeleton," J. Neuroeng. Rehabil., **16**(1), pp. 1–13.
[15] Simo, L., Botzer, L., Ghez, C., and Scheidt, R. A., 2014, "A Robotic Test of Proprioception Within the Hemiparetic Arm Post-Stroke," J. Neuroeng. Rehabil., **11**(1), pp. 1–12.
[16] Rinderknecht, M. D., Lambercy, O., Raible, V., Büsching, I., Sehle, A., Liepert, J., and Gassert, R., 2018, "Reliability, Validity, and Clinical Feasibility of a Rapid and Objective Assessment of Post-Stroke Deficits in Hand Proprioception," J. Neuroeng. Rehabil., **15**(1), pp. 1–15.
[17] Zhou, Z., Zhou, Y., Wang, N., Gao, F., Wei, K., and Wang, Q., 2015, "A Proprioceptive Neuromuscular Facilitation Integrated Robotic Ankle-Foot System for Post Stroke Rehabilitation," Rob. Auton. Syst., **73**, pp. 111–122.
[18] Sanguineti, V., Casadio, M., Vergaro, E., Squeri, V., Giannoni, P., and Pg, M., 2009, "Robot Therapy for Stroke Survivors: Proprioceptive Training and Regulation of Assistance," Stud. Health Technol. Inf., **145**, pp. 126–142.
[19] Reinsdorf, D., Mahan, E., and Reinkensmeyer, D., 2021, "Proprioceptive Gaming: Making Finger Sensation Training Intense and Engaging With the P-Pong Game and PINKIE Robot," 2021 43rd Annual International Conference of the IEEE Engineering in Medicine and Biology Society (EMBC), Guadalajara, Mexico, Oct. 31–Nov. 4, pp. 6715–6720.
[20] Taheri, H., Rowe, J. B., Gardner, D., Chan, V., Gray, K., Bower, C., Reinkensmeyer, D. J., and Wolbrecht, E. T., 2014, "Design and Preliminary Evaluation of the FINGER Rehabilitation Robot: Controlling Challenge and Quantifying Finger Individuation During Musical Computer Game Play," J. Neuroeng. Rehabil., **11**(1), pp. 1–17.
[21] Ingemanson, M. L., Rowe, J. B., Chan, V., Wolbrecht, E. T., Cramer, S. C., and Reinkensmeyer, D. J., 2016, "Use of a Robotic Device to Measure Age-Related Decline in Finger Proprioception," Exp. Brain Res., **234**(1), pp. 83–93.
[22] Ingemanson, M. L., Rowe, J. R., Chan, V., Wolbrecht, E. T., Reinkensmeyer, D. J., and Cramer, S. C., 2019, "Somatosensory System Integrity Explains Differences in Treatment Response After Stroke," Neurology, **92**(10), pp. E1098–E1108.
[23] Chung, K. C., and Wei, F. C., 2000, "An Outcome Study of Thumb Reconstruction Using Microvascular Toe Transfer," J. Hand Surg., **25**(4), pp. 651–658.
[24] Segu, S. S., Athavale, S. N., and Manjunath, P., 2015, "Osteoplastic Reconstruction for Post Traumatic Thumb Amputations Around Metacarpophalangeal Joint," J. Clin. Diagn. Res., **9**(8), pp. 11–13.
[25] Li, J., Zheng, R., Zhang, Y., and Yao, J., 2011, "iHandRehab: An Interactive Hand Exoskeleton for Active and Passive Rehabilitation," 2011 IEEE International Conference on Rehabilitation Robotics, ETH Zurich Science City, Switzerland, June 29–July 1, pp. 1–6.
[26] Ueki, S., Kawasaki, H., Ito, S., Nishimoto, Y., Abe, M., Aoki, T., Ishigure, Y., Ojika, T., and Mouri, T., 2012, "Development of a Hand-Assist Robot With Multi-Degrees-of-Freedom for Rehabilitation Therapy," IEEE/ASME Trans. Mechatron., **17**(1), pp. 136–146.

[27] Bouzit, M., Burdea, G., Popescu, G., and Boian, R., 2002, "The Rutgers Master II—New Design Force-Feedback Glove," IEEE/ASME Trans. Mechatron., **7**(2), pp. 256–263.
[28] Polygerinos, P., Wang, Z., Galloway, K. C., Wood, R. J., and Walsh, C. J., 2015, "Soft Robotic Glove for Combined Assistance and at-Home Rehabilitation," Rob. Auton. Syst., **73**, pp. 135–143.
[29] Yap, H. K., Lim, J. H., Nasrallah, F., and Yeow, C. H., 2017, "Design and Preliminary Feasibility Study of a Soft Robotic Glove for Hand Function Assistance in Stroke Survivors," Front. Neurosci., **11**, p. 547.
[30] Maciejasz, P., Eschweiler, J., Gerlach-Hahn, K., Jansen-Troy, A., and Leonhardt, S., 2014, "A Survey on Robotic Devices for Upper Limb Rehabilitation," J. Neuroeng. Rehabil., **11**(1), pp. 1–29.
[31] Suarez-Escobar, M., and Rendon-Velez, E., 2018, "An Overview of Robotic/Mechanical Devices for Post-Stroke Thumb Rehabilitation," Disabil. Rehabil. Assistive Technol., **13**(7), pp. 683–703.
[32] Wang, F., Shastri, M., Jones, C. L., Gupta, V., Osswald, C., Kang, X., Kamper, D. G., and Sarkar, N., 2011, "Design and Control of an Actuated Thumb Exoskeleton for Hand Rehabilitation Following Stroke," 2011 IEEE International Conference on Robotics and Automation, Shanghai, China, May 9–13, pp. 3688–3693.
[33] Aiple, M., and Schiele, A., 2013, "Pushing the Limits of the CyberGrasp™ for Haptic Rendering," 2013 IEEE International Conference on Robotics and Automation, Karlsruhe, Germany, May 6–10, pp. 3541–3546.
[34] Takagi, M., Iwata, K., Takahashi, Y., Yamamoto, S. I., Koyama, H., and Komeda, T., 2009, "Development of a Grip Aid System Using Air Cylinders," 2009 IEEE International Conference on Robotics and Automation, Kobe, Japan, May 12–17, pp. 2312–2317.
[35] Burton, T. M. W., Vaidyanathan, R., Burgess, S. C., Turton, A. J., and Melhuish, C., 2011, "Development of a Parametric Kinematic Model of the Human Hand and a Novel Robotic Exoskeleton," 2011 IEEE International Conference on Rehabilitation Robotics, ETH Zurich Science City, Switzerland, June 29–July 1, pp. 1–7.
[36] Agarwal, P., Yun, Y., Fox, J., Madden, K., and Deshpande, A. D., 2017, "Design, Control, and Testing of a Thumb Exoskeleton With Series Elastic Actuation," Int. J. Rob. Res., **36**(3), pp. 355–375.
[37] Cantero-Téllez, R., and Medina Porqueres, I., 2021, "Practical Exercises for Thumb Proprioception," J. Hand Ther., **34**(3), pp. 488–492.
[38] Mathiowetz, V., Volland, G., Kashman, N., and Weber, K., 1985, "Adult Norms for the Box and Block Test of Manual Dexterity," Am. J. Occup. Ther., **39**(6), pp. 386–391.
[39] Samson, E., Laurendeau, D., Parizeau, M., Comtois, S., Allan, J. F., and Gosselin, C., 2006, "The Agile Stereo Pair for Active Vision," Mach. Vision Appl., **17**(1), pp. 32–50.
[40] Jiang, M., Hu, X., Liu, L., and Yu, Y., 2012, "Study on Parallel 2-DOF Rotation Mechanism in Radar," Phys. Procedia, **24**, pp. 1830–1835.
[41] Lum, M. J. H., Rosen, J., Sinanan, M. N., and Hannaford, B., 2004, "Kinematic Optimization of a Spherical Mechanism for a Minimally Invasive Surgical Robot," Proceedings of the 2004 IEEE International Conference on Robotics and Automation, ICRA'04, New Orleans, LA, Apr. 26–May 1, pp. 829–834.
[42] Hsieh, H. C., Chen, D. F., Chien, L., and Lan, C. C., 2017, "Design of a Parallel Actuated Exoskeleton for Adaptive and Safe Robotic Shoulder Rehabilitation," IEEE/ASME Trans. Mechatron., **22**(5), pp. 2034–2045.
[43] Palmieri, G., 2015, "On the Positioning Error of a 2-DOF Spherical Parallel Wrist With Flexible Links and Joints—An FEM Approach," Mech. Sci., **6**(1), pp. 9–14.
[44] Danaei, B., Arian, A., Tale Masouleh, M., and Kalhor, A., 2017, "Dynamic Modeling and Base Inertial Parameters Determination of a 2-DOF Spherical Parallel Mechanism," Multibody Syst. Dyn., **41**(4), pp. 367–390.
[45] Cervantes-Sánchez, J., Hernández-Rodríguez, J., and González-Galván, E. J., 2004, "On the 5R Spherical, Symmetric Manipulator: Workspace and Singularity Characterization," Mech. Mach. Theory, **39**(4), pp. 409–429.
[46] Ouerfelli, M., and Kumar, V., 1994, "Optimization of a Spherical Five-Bar Parallel Drive Linkage," ASME J. Mech. Des., **116**(1), pp. 166–173.
[47] Heidari, O., Wolbrecht, E. T., Perez-Gracia, A., and Yihun, Y. S., 2018, "A Task-Based Design Methodology for Robotic Exoskeletons," J. Rehabil. Assistive Technol. Eng., **5**, pp. 1–12.
[48] Choi, W. H., and Takeda, Y., 2021, "Geometric Design and Prototyping of a (2-RRU)-URR Parallel Mechanism for Thumb Rehabilitation Therapy," Machines, **9**(3), p. 50.
[49] Zapatero-Gutiérrez, A., Castillo-Castañeda, E., and Laribi, M. A., 2021, "On the Optimal Synthesis of a Finger Rehabilitation Slider-Crank-Based Device With a Prescribed Real Trajectory: Motion Specifications and Design Process," Appl. Sci. (Switzerland), **11**(2), pp. 708–724.
[50] Murray, R. M., Li, Z., and Sastry, S., 1994, *A Mathematical Introduction to Robotic Manipulation*, CRC Press, Boca Raton, FL.
[51] Aguirre-Ollinger, G., Colgate, J. E., Peshkin, M. A., and Goswami, A., 2011, "Design of an Active One-Degree-of-Freedom Lower-Limb Exoskeleton With Inertia Compensation," Int. J. Rob. Res., **30**(4), pp. 486–499.